

LA-UR- 00 - 3110

Approved for public release;  
distribution is unlimited.

*Title:* ELECTROCHEMICALLY-GROWN OXIDES ON U-NB  
ALLOY

*Author(s):* Jennifer A. Lillard  
Daniel N. Kelly  
Mark T. Paffett  
Robert J. Hanrahan

*Submitted to:* To be published in Proceedings Volume for 197th Meeting  
of the Electrochemical Society

## Los Alamos

NATIONAL LABORATORY

Los Alamos National Laboratory, an affirmative action/equal opportunity employer, is operated by the University of California for the U.S. Department of Energy under contract W-7405-ENG-36. By acceptance of this article, the publisher recognizes that the U.S. Government retains a nonexclusive, royalty-free license to publish or reproduce the published form of this contribution, or to allow others to do so, for U.S. Government purposes. Los Alamos National Laboratory requests that the publisher identify this article as work performed under the auspices of the U.S. Department of Energy. Los Alamos National Laboratory strongly supports academic freedom and a researcher's right to publish; as an institution, however, the Laboratory does not endorse the viewpoint of a publication or guarantee its technical correctness.

## **DISCLAIMER**

**This report was prepared as an account of work sponsored by an agency of the United States Government. Neither the United States Government nor any agency thereof, nor any of their employees, make any warranty, express or implied, or assumes any legal liability or responsibility for the accuracy, completeness, or usefulness of any information, apparatus, product, or process disclosed, or represents that its use would not infringe privately owned rights. Reference herein to any specific commercial product, process, or service by trade name, trademark, manufacturer, or otherwise does not necessarily constitute or imply its endorsement, recommendation, or favoring by the United States Government or any agency thereof. The views and opinions of authors expressed herein do not necessarily state or reflect those of the United States Government or any agency thereof.**

## **DISCLAIMER**

**Portions of this document may be illegible in electronic image products. Images are produced from the best available original document.**

# ELECTROCHEMICALLY-GROWN OXIDES ON U-Nb ALLOYS

J.A. Lillard, D.N. Kelly\*, M.T. Paffett\*, R.J. Hanrahan

Materials Corrosion & Environmental Effects Laboratory  
Materials Science & Technology Division, MS G755

Los Alamos National Laboratory

Los Alamos, NM 87545

\*Chemistry Division

RECEIVED

NOV 13 2000

OSTI

## ABSTRACT

Electrochemically-grown oxides on U-Nb alloys (2 – 8 wt. %) were mixed oxides consisting of varying amounts of  $\text{Nb}_2\text{O}_5$ ,  $\text{UO}_3 \cdot 2\text{H}_2\text{O}$ , and  $\text{UO}_2$ . Nb enhanced the passivity of U in acidic and neutral solutions through the formation of  $\text{Nb}_2\text{O}_5$  and enrichment of Nb in the oxide. In highly acidic solutions, where U did not form a solid oxide, Nb additions greater than 8 % would be required to achieve passivity. In alkaline solutions Nb did not significantly increase the passivity of the mixed oxide and there was no enrichment of Nb. U-8Nb, which had a lower  $i_{\text{PASS}}$  than Nb or U in pH 10.7 solution, was the exception; the behavior is thought to be due to the unique U-8Nb phase structure. In highly alkaline solutions, Nb was shown to be an ineffective alloy element for promoting passivity because, although it formed  $\text{Nb}_2\text{O}_5$ , the oxide was non-protective.

## INTRODUCTION

Depleted uranium (U) is attractive as an engineering material because of its high density ( $\rho_{\text{U}} = 1.7\rho_{\text{Pb}}$ ). Poor corrosion resistance limits its use, however. Test data show that alloying with niobium (Nb) increases corrosion resistance; the increase depends on the amount of Nb added and additions of 6 wt. % Nb provide good corrosion resistance (1, 2). There is a large difference between the melting temperatures of U and Nb ( $\Delta T = 1340^\circ\text{C}$ ) (3), and it is therefore difficult to achieve an ingot that has a homogeneous distribution of Nb. Spatial variation in Nb concentration causes structures made from the ingot to have spatial variations in corrosion resistance.

Nb concentration can affect both the microstructure of the alloy and the chemical makeup of the oxide. The phase structure of U-Nb alloys varies from a distortion of the orthorhombic, room-temperature phase ( $\alpha$ ) for U-2Nb to a distortion of the bcc, high-temperature phase ( $\gamma$ ) for U-8Nb (4). The composition of the oxide (e.g., ratio of U oxide to Nb oxide) will likely depend on the amount of Nb in the alloy. The objectives of this work were to characterize electrochemically-grown oxides of U-Nb alloys using electrochemical and surface science methods and to compare them to those of pure Nb and U in order to assess the role of Nb.

DRAFT

1/12

## EXPERIMENTAL

Oxides were studied in deaerated solutions ranging in pH from 0.5 to 13.6 on U, Nb, and U-Nb alloys ranging from 2% to 8% Nb by weight. Electrochemical passivation was examined using potentiodynamic polarization. Oxide composition after potentiostatic anodic film growth was examined using X-ray photoelectron spectroscopy.

### Material

U-Nb alloys with 2%, 4%, 6%, and 8% Nb additions by weight were examined. Small buttons of the alloys, approximately 4 cm in diameter, were fabricated to ensure homogeneous Nb distribution. The as-cast buttons were solutionized at 800 °C and then water quenched to room temperature. Depleted U and Nb samples were also examined for comparison to the alloys.

### Polarization Studies

Potentiodynamic polarization scans were performed to measure the room-temperature, electrochemical behavior of the U-Nb alloys in a variety of acidic and basic solutions. Solutions were made using 18.2 M $\Omega$ -cm water and reagent grade chemicals; the exact pH values and solution compositions are shown in Table I. All solutions were deaerated with argon for at least 6 h before, as well as during, the experiment. Scans were performed at 0.17 mV/s using a conventional three-electrode glass cell. The scans were started 0.03 V below the open circuit potential ( $E_{OC}$ ), stopped at a specified potential, and then reversed to  $E_{OC}$ . The counter electrode material was plantinized niobium mesh. A mercury-mercury sulfate reference electrode was used, but all potentials are referenced against the saturated calomel electrode (SCE). Working electrodes were made from rectangular pieces (approximately 2 cm by 1 cm) of the U-Nb alloys. Electrical leads were attached to the pieces. The samples were then mounted in epoxy, and the leads were encased in glass rods. The mounted samples were ground to 800 grit SiC and degreased in ethanol just prior to testing. A polyester-based tape with a silicone adhesive was used to mask a known area of the sample and prevent crevice corrosion.

Table I. pH and composition of solutions used in electrochemical experiments.

pH	Composition
0.5	0.5 M Sulfuric Acid
4.0	0.5 M Boric Acid
7.2	0.5 M Boric Acid + 0.05 M Sodium Borate
10.7	0.05 M Sodium Hydroxide + 0.025 M Sodium Borate
13.6	0.5 M Potassium Hydroxide

### Surface Science

Prior to surface science analysis, oxides were electrochemically grown on samples. Unmounted samples were prepared to a surface finish of 1- $\mu$ m diamond. An electrical lead was attached to the back of the sample with silver paint; epoxy was used to insulate the lead from solution. Samples were tested as in the polarization studies except that instead of potentiodynamic polarization, potentiostatic polarization was performed. For this study, samples were polarized to 0.6 V<sub>SCE</sub> until the current reached steady-state (typically one hour). After the electrochemical treatment samples were transported to a vacuum chamber where the surface science analysis was performed.

X-ray photoelectron spectroscopy (XPS) and sputtered neutrals mass spectrometry (SNMS) experiments were performed in an ultra-high vacuum chamber with a base pressure typically below  $2 \times 10^{-10}$  Torr. The XPS data were obtained using a non-monochromatic Mg K $\alpha$  x-ray source ( $h\nu = 1253.6$  eV) and the photoemitted electrons were energy sorted using a hemispherical analyzer. All XPS data were taken with the plane of the sample surface perpendicular to the analyzer axis (zero take-off angle). Pass energies were typically 29 eV and incident x-ray power was 250 W. XP spectra are reported here in terms of binding energy (BE) and are referenced in all cases to a peak position of 284.6 eV for adventitious carbon. The SNMS data were acquired using a differentially pumped 5 keV Xe $^+$  ion beam passed through a Wein filter rastered over a 2 mm by 2 mm area. Depth profiling was performed using an ion beam fluence that corresponds to a sputter removal rate of approximately 30 Å/min from thin oxides on U-Nb alloys. All XPS and SNMS data were collected at sample temperatures of approximately 300 K.

Prior XPS work on the oxidation of U-Nb alloys indicates the facile thermal formation of stoichiometric UO $_2$  upon oxygen exposure at room temperature (5). The U4f $_{7/2}$  peak of stoichiometric UO $_2$  can be well fit by a single peak at 380.0 eV (6). Shakeup peaks at 6.9 eV higher than the predominant U4f $_{7/2}$  and U4f $_{5/2}$  features further verify the formation of stoichiometric UO $_2$  (6). In the electrochemically oxidized samples, we typically observed two peaks in the U4f $_{7/2}$  region, one at a binding energy of 380.0 eV, and another arising at a binding energy of 381.8 eV, which is indicative of UO $_3(\cdot 2H_2O)$  formation (6). Also, the observance and intensity of the peak at 381.8 eV generally correlated with diminished intensity of shakeup features, as expected for UO $_3(\cdot 2H_2O)$  formation. Hence, we have deconvoluted the U4f $_{7/2}$  XPS peak for each of the samples by fitting this spectral region using two peaks with constant a full-width half-maximum of 2 eV and Gaussian/Lorentzian ratios at binding energies of 381.8 eV and 380.0 eV. This allows determination the ratio of uranium extant in each sample as UO $_3(\cdot 2H_2O)$  and UO $_2$ . Contributions to the U4f XPS peaks from hyperstoichiometric UO $_{2+x}$ , evident in the spectra by additional shakeup features, are quantified during fitting by the 380.0 eV binding energy peak.

## RESULTS

### Potentiodynamic Polarization

Overall, the addition of Nb generally enhanced passivity in acidic and neutral solutions as measured by anodic potentiodynamic polarization scans. Passive current density ( $i_{PASS}$ ) decreased as alloy content increased, and  $i_{PASS}$  was similar for U-8Nb and Nb. Positive hysteresis during the reverse scan indicated that the film formed on U was not protective in these solutions. The U-Nb alloys, particularly U-2Nb and U-4Nb, formed only minimally protective films in the pH 0.5 and 4.0 solutions. Nb additions produced a less significant effect in alkaline solutions. Negative hysteresis during reverse scans showed that all samples had protective films in pH 10.7 solution. In the pH 13.6 solution, none of the samples formed significantly protective films.

Nb exhibited passive behavior at all pH values tested except for the pH 13.6 solution (Figure 1). In pH 13.6 solution, Nb had an active nose that was followed by a region of limited, but high, current density, which suggests that a film formed but it was not

protective. This limiting current density will be referred to as, " $i_{\text{LIMITING}}$ ." Small active noses were observed at the other pH values. The potential at the onset of transpassive dissolution decreased as pH increased and was above the reversible potential for oxygen evolution for all solutions.

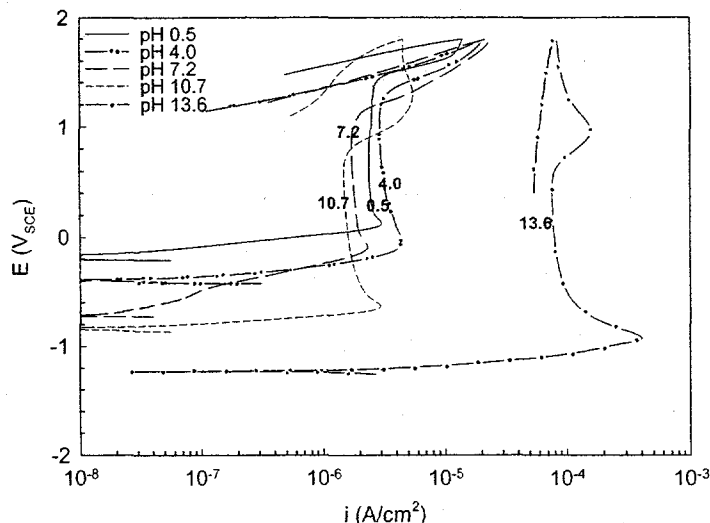


**Figure 1.** Anodic polarization scans of Nb as a function of pH in deaerated solutions. Complete reverse scan data are not shown for clarity.

Anodic polarization scans of U in various pH solutions shows that only at pH 10.7 was U passive over the entire potential range studied (Figure 2). It also appears that there were several regions with unique potential and current density ( $E$ - $i$ ) behavior. The first region occurred between  $E_{\text{OC}}$  and about  $0 V_{\text{SCE}}$ . A second region occurred above  $0 V_{\text{SCE}}$ , and in some cases, a third region, transpassive behavior, was observed. In the first  $E$ - $i$  region, U was passive as determined by the current density and negative hysteresis of the reverse scan. In the second region, passive behavior was only observed in pH 10.7 solution; at pH values above and below 10.7 current density was  $>10 \mu\text{A}/\text{cm}^2$  and hysteresis was zero or positive.

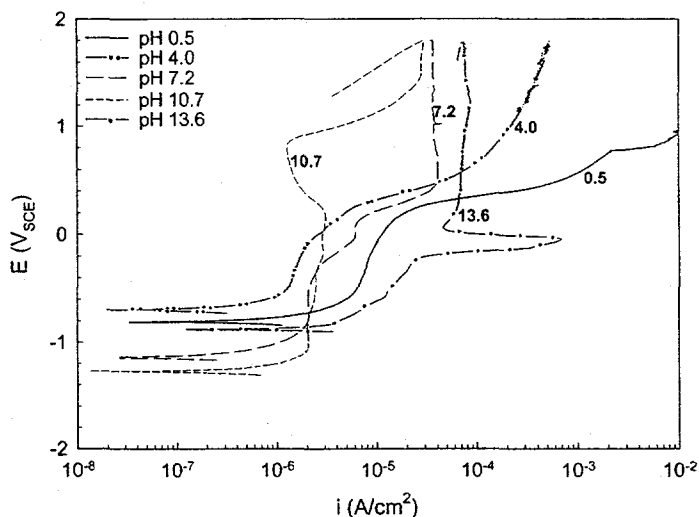


**Figure 2.** Anodic polarization scans of U as a function of pH in deaerated solutions. Complete reverse scan data are not shown for clarity.

In acidic solutions, Nb alloy additions of 2-8 wt. % increased the corrosion resistance of U as measured by polarization scans.  $E_{OC}$  of the alloys was higher than that of U and was closer to  $E_{OC}$  of Nb; corrosion current density of the alloys was lower than U and generally decreased as Nb content increased. The Nb additions, however, did not always promote passive oxide formation in acidic solutions. The polarization scans for U, Nb, and the U-Nb alloys in pH 4.0 solution show that only Nb and U-8Nb formed passive films over the entire potential region studied (Figure 3).

The shapes of the polarization curves in Figure 3 were different for Nb as compared to U and the alloys. Nb exhibited a very small active nose and then one region of passivity, while U and the alloys showed no active nose but appeared to have two E-i regions where current density was limited. In the first region, between  $E_{OC}$  and about  $0.3 V_{SCE}$ , the current density was less than  $10 \mu A/cm^2$  and increased somewhat as E increased. The alloys' values of  $i_{PASS}$  in this region were similar but smaller than the value for U. In the second region,  $E \geq 0.3 V_{SCE}$ ,  $i_{LIMITING}$  values were higher and increased as Nb content decreased. Only Nb and U-8Nb showed passive behavior ( $i$  less than  $10 \mu A/cm^2$ ). U-4Nb, U-6Nb, and U-8Nb showed very small active noses during the transition from the first to the second regions. Reverse scans showed negative hysteresis in the first, low E-i region for all materials except U. In the second region, only U-8Nb and Nb showed negative hysteresis. As the figure shows, the hysteresis for Nb was much larger than that of U-8Nb. Polarization scans in pH 0.5 solution were similar to those in pH 4.0 except that U and the alloys showed active behavior above  $0.3 V_{SCE}$  instead of a second region of film formation.

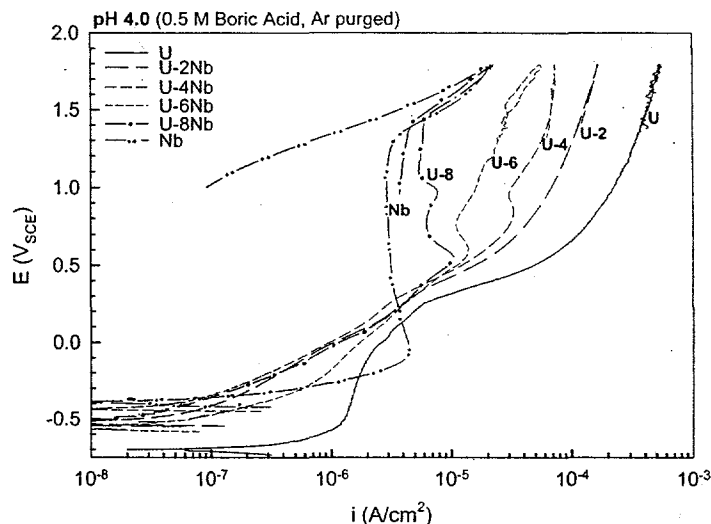


**Figure 3.** Anodic polarization scans for U, Nb, and U-Nb alloys in deaerated pH 4.0 boric acid solution. The data for the reverse scans are not shown for clarity.

In pH 7.2 solution, Nb significantly enhanced the passivity of the U-Nb alloys (Figure 4). Nb additions increased  $E_{OC}$  and lowered current densities to  $<10 \mu A/cm^2$ . In the low E-i region, current densities were similar to those of Nb. In the high E-i region,  $i_{PASS}$  decreased as Nb content increased, and  $i_{PASS}$  of U-8Nb was about equal to that of Nb. Transpassive behavior was observed above the reversible potential for oxygen evolution. U showed similar behavior to acidic solutions – multiple regions of E-i behavior with only the low E-i region exhibiting passive characteristics.

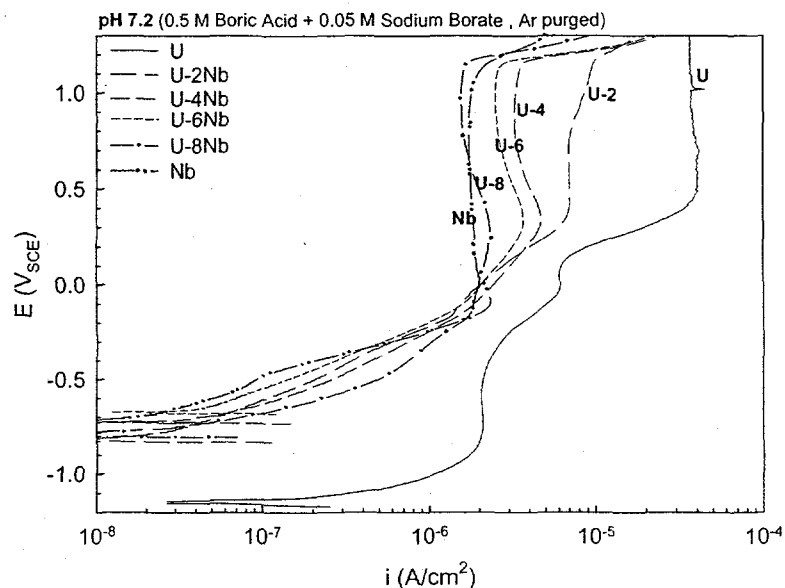


**Figure 4.** Anodic polarization scans for U-Nb alloys in deaerated pH 7.2 borate buffer solution. Reverse scan data are not shown for clarity.

The potentiodynamic behavior of U and the U-Nb alloys compared to Nb in pH 10.7 solution was different from the neutral and acidic solutions (Figure 5). While the addition of Nb to U increased  $E_{OC}$  as it did in the other solutions, the alloys and U obtained lower  $i_{PASS}$  than Nb. In particular, the  $i_{PASS}$  of U-8Nb was lower than either Nb or U over nearly the entire potential range. Similar behavior of U and the alloys was observed in pH 13.6 solution. However, non-protective films formed with limiting current densities on the order of  $100 \mu\text{A}/\text{cm}^2$ .

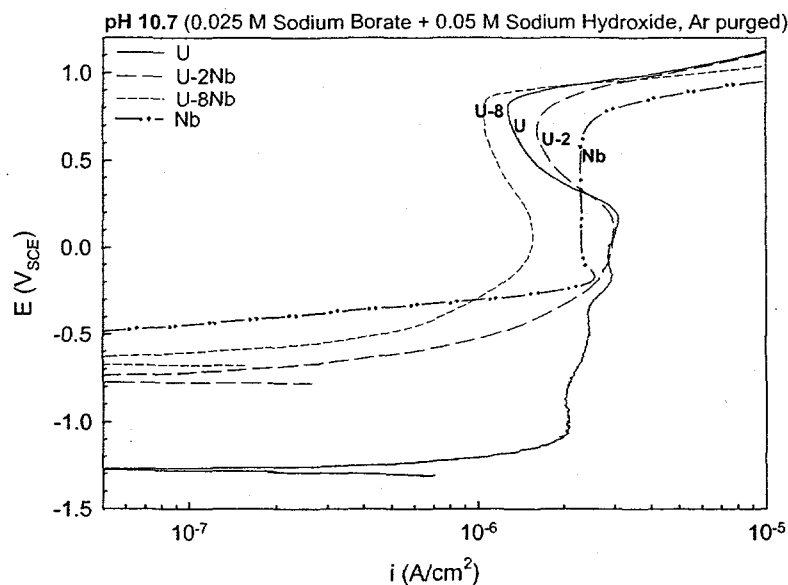


**Figure 5.** Anodic polarization scans for various U-Nb alloys in deaerated pH 10.7 borate-hydroxide solution. Reverse scan data and data for U-4Nb and U-6Nb are not shown for clarity.

In order to compare the complete set of data, the limiting current densities of the high E-i regions were plotted as a function of pH and Nb alloy content (Figure 6). For the test conditions that produced anodic films, pH 4.0 through pH 13.6, the limiting current density (either  $i_{PASS}$  or  $i_{LIMITING}$ ) was plotted. In pH 0.5 solution, U and the alloys were active. For comparative purposes, the current at 0.75  $V_{SCE}$  was plotted for this solution instead of the limiting current and the data were marked "active." The graph shows that in mildly acidic and neutral solutions, Nb additions enhance passivity as measured by  $i_{PASS}$ . It also shows that slightly lower  $i_{PASS}$  may be achieved for solutions around pH 4 by increasing the Nb content of the alloy above 8 wt. %. In very acidic solutions, there is a possibility that Nb additions could promote passivity, but a much greater amount than 8 wt. % would be required. In basic solutions, Nb did little to enhance passivity or corrosion resistance.

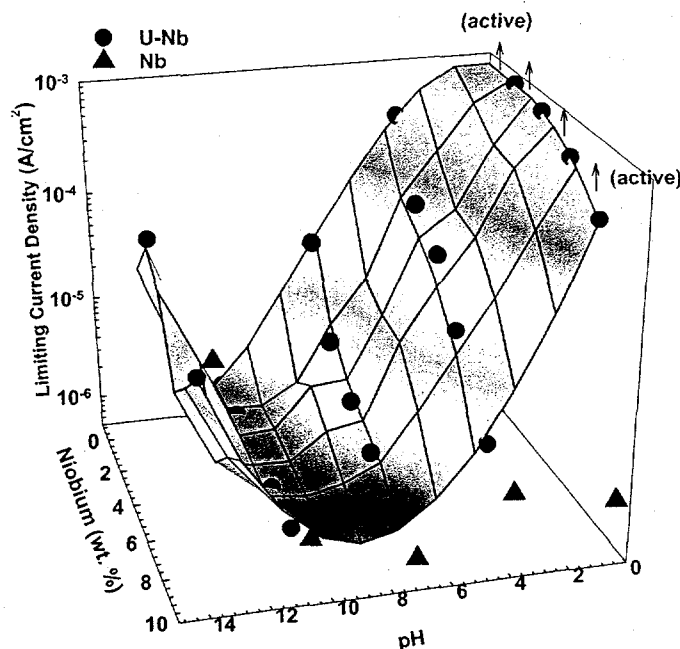


Figure 6. Anodic limiting current density as a function of pH and bulk Nb concentration.

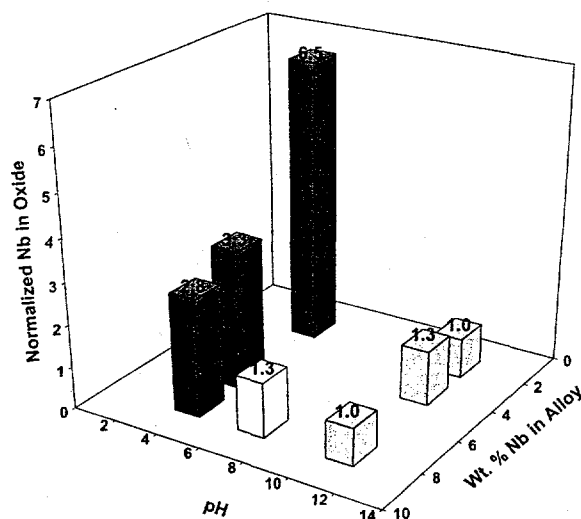
### Surface Science

Table II shows XPS results for U-Nb alloys as a function of bulk Nb concentration and solution pH. XPS was used to characterize the weight percent of Nb in the near-surface region (outermost 50-70 Å) of the samples, as well as to determine the relative amounts of U attributed to  $UO_3 \cdot 2H_2O$  and  $UO_2$  valence states, through deconvolution of the  $U4f_{7/2}$  peak as explained in the Experimental section. For all samples tested, XPS indicated that surface niobium was oxidized to  $Nb_2O_5$ . Because SNMS data were taken over several months, quantitative thickness cannot be compared. However, SNMS data qualitatively show that oxides grown under conditions that showed passive behavior (e.g., U-2Nb, pH 10.7, 0.6  $V_{SCE}$ ) were significantly thinner than those where non-protective films formed (e.g., U-2Nb, pH 4, 0.6  $V_{SCE}$ ). Furthermore, when the polarization time under which the non-protective films were grown was increased (e.g., U-2Nb at pH 4, 2h vs 1h), significantly thicker oxides were observed.

**Table II.** Near-surface Nb wt. % and  $\text{UO}_3 \cdot (2\text{H}_2\text{O})$  character of electrochemically oxidized U-Nb alloys.

Alloy	pH	Nb Wt. % (near-surface)	At. % $\text{UO}_3 \cdot (2\text{H}_2\text{O})$
U-8Nb	10.7	7.3	90
	7.2	10.8	78
	4.0	22.6	67
U6Nb	4.0	19.9	66
U4Nb	10.7	5.3	80
U2Nb	10.7	1.9	32
	4.0	13.3	50 (1 h), 85 (2 h)
Depleted Uranium	10.7	--	25

The enhancement of Nb in the near-surface region with decreasing solution pH is shown graphically in Figure 7. At pH 4.0, there was greater than a factor of six increase in the Nb weight percent at the surface relative to that in the bulk for U-2Nb. The Nb enhancement factor decreased as Nb alloy content increased: for U-8Nb the factor was 2.8. In neutral and basic solutions, however, there was little to no enhancement of Nb in the oxide. Such results indicate a selective dissolution of U relative to Nb from the alloy surface with decreasing pH. Surface sensitive angle-resolved XPS measurements of several samples, obtained at take-off angles of  $60^\circ$ , showed even greater Nb enhancements than those obtained with a  $0^\circ$  take-off angle, which further suggests dissolution of uranium from the alloy surface region. For instance, the near-surface Nb wt. % for U-8Nb at pH 7.2 was 13% at a take-off angle of  $60^\circ$ , compared to 10.8% at a take-off angle of  $0^\circ$ .



**Figure 7.** Enrichment of Nb in the oxide, normalized to Nb bulk concentration, as a function of solution pH and Nb alloy content.

Figure 8 shows a representative XP spectrum of the  $\text{U}4f_{7/2}$  region, shown specifically for U-8Nb polarized at 0.6  $\text{V}_{\text{SCE}}$  in pH 10.7 solution. The figure illustrates the contributions to the XPS peak arising from  $\text{UO}_3 \cdot (2\text{H}_2\text{O})$  and  $\text{UO}_2$ , corresponding to the deconvoluted curves at binding energies of 381.8 eV and 380.0 eV, respectively. For this

sample, deconvolution of the  $U4f_{7/2}$  peak indicates the U oxide layer was 90 atomic %  $UO_3 \cdot (2H_2O)$  and 10%  $UO_2$ . The deconvolution of angle-resolved XPS measurements gave ratios of  $UO_3 \cdot (2H_2O)/UO_2$  that were identical for all samples of Table II, indicating that these two valence states were well-mixed in the oxide layer. Also note that  $UO_3 \cdot (2H_2O)$  was reduced to  $UO_2$  in air, atomic hydrogen, x-rays, and even long exposures to vacuum.

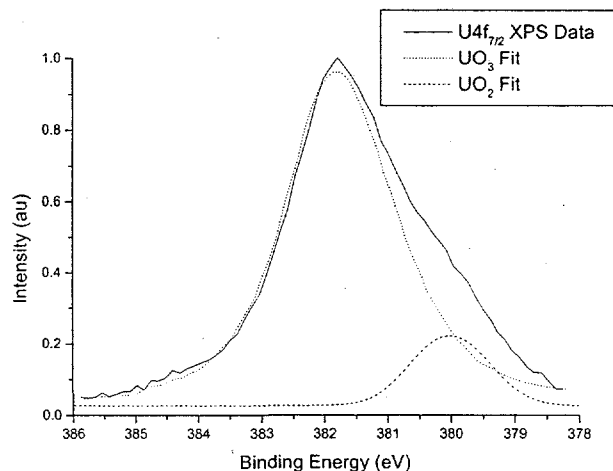


**Figure 8.** The  $U4f_{7/2}$  XPS peak of U-8Nb, which was polarized at 0.6  $V_{SCE}$  in pH 10.7 solution. Shown is the original XPS linescan and the deconvoluted peaks at BE of 381.8 eV ( $UO_3 \cdot (2H_2O)$ ) and 380.0 eV ( $UO_2$ ).

Figure 9 indicates a relationship between pH, bulk Nb concentration, and U valence state for electrochemically-grown oxides. For U-8Nb, the  $UO_3 \cdot (2H_2O)$ -like character of the oxide increased with increasing pH. However, for U-2Nb, the  $UO_3 \cdot (2H_2O)$ -like character of the oxide decreased with increasing pH. At pH 10.7, the  $UO_3 \cdot (2H_2O)$  content of the oxide increased as Nb alloy content increased, but at pH 4, the  $UO_3 \cdot (2H_2O)$  content was similar for all the alloys.

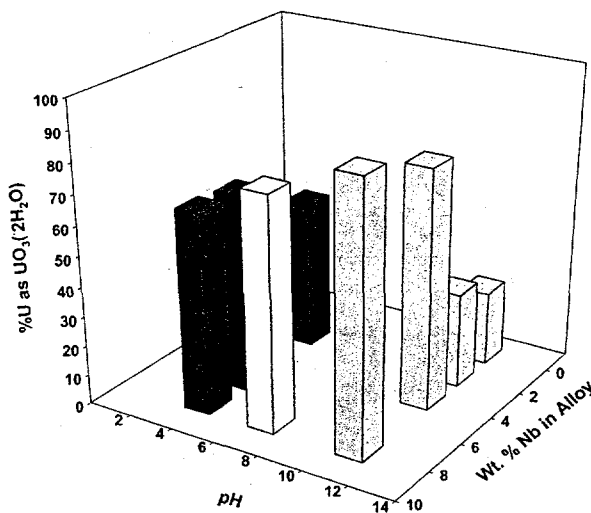


**Figure 9.** Percentage of U as  $UO_3 \cdot (2H_2O)$  in electrochemically-grown oxides on U-Nb alloys.

## DISCUSSION

In general, the results showed that alloying with Nb improved the corrosion resistance of U for a variety of solution pH's. The results also raised four questions for discussion:

- 1) How did Nb change the corrosion resistance of U oxides in acids vs bases?
- 2) What caused the multiple regions of E-i behavior observed for U and U-Nb alloys?
- 3) Why did the  $\text{UO}_3 \cdot (2\text{H}_2\text{O})$  character vary with pH and Nb alloy content?
- 4) Why was  $i_{\text{PASS}}$  lower for U-8Nb than for either U or Nb in basic solutions?

Potentiodynamic polarization showed that both U and Nb exhibited passive and non-passive behavior over the pH range 0.5 to 13.6. The two metals also showed multiple regions of E-i behavior. Pourbaix diagrams (7) for U and Nb (Figure 10) show that U and Nb undergo several changes in valance as potential is increased. These valence changes (e.g.,  $\text{UO}_2 / \text{UO}_3 \cdot (2\text{H}_2\text{O})$ ) roughly correspond to the potentials where changes in the E-i behavior were observed. The diagrams also indicate that solid oxides of Nb are thermodynamically stable over the entire pH range; however, solid oxides of U are not and U should dissolve in acidic solutions. Potentiodynamic polarization scans indicated anodic dissolution of U for both U and U-Nb alloys in pH 0.5 solution. Furthermore, U oxides that formed in pH 4 solution typically did not provide passivity (Figure 3). Polarization scans of Nb indicated oxide formation at all pH values, but the high limiting current density of Nb in pH 13.6 solution suggests that the oxide is non-protective in highly alkaline solutions (Figure 1).

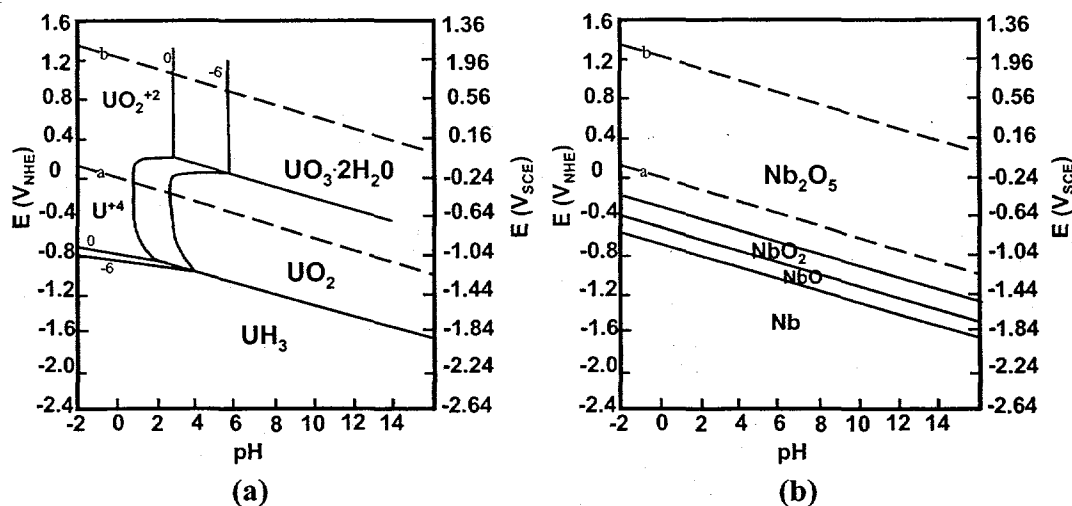


Figure 10. Pourbaix diagrams for (a) U and (b) Nb (7).

In most cases, the U-Nb alloys exhibited the combined passive and non-passive behavior, as well as multiple regions of E-i behavior, of U and Nb. XPS after potentiostatic polarization at 0.6 V<sub>SCE</sub> in solutions of pH 4 to 10.7 showed that a mixed oxide formed on the U-Nb alloys. Nb was found as  $\text{Nb}_2\text{O}_5$ , and Nb was enriched compared to the alloy content in acidic solutions. U was found as  $\text{UO}_3 \cdot (2\text{H}_2\text{O})$  and  $\text{UO}_2$ . There was no enrichment of U, and the amount of  $\text{UO}_3 \cdot (2\text{H}_2\text{O})$  vs  $\text{UO}_2$  varied with pH and Nb alloy content.

Nb enrichment in the oxide in acidic solution is expected given that U dissolution is thermodynamically favorable at low pH and low U ion solution concentrations. A likely scenario for Nb oxide enrichment at pH 4 is that U dissolves and  $\text{Nb}_2\text{O}_5$  forms until the near-surface concentration of U ions in solution reaches the critical value for  $\text{UO}_3 \cdot (2\text{H}_2\text{O})$  to form. At this point  $\text{UO}_3 \cdot (2\text{H}_2\text{O})$  and  $\text{Nb}_2\text{O}_5$  form, which results in an oxide that is enriched in Nb.

The Pourbaix diagrams (Figure 10) predict  $\text{Nb}_2\text{O}_5$  and  $\text{UO}_3 \cdot (2\text{H}_2\text{O})$  should be the only solid oxides formed under the test conditions. However, all of the mixed oxides showed  $\text{UO}_2$  formation. In air  $\text{UO}_2$  is the stable form of the oxide, and XPS analysis found that air, atomic hydrogen, x-rays, and even long exposures to vacuum reduced  $\text{UO}_3 \cdot (2\text{H}_2\text{O})$  to  $\text{UO}_2$ . It is likely that reduction of the oxide in air is the primary reason  $\text{UO}_2$  was found in all of the U-Nb alloys. Even though samples were transferred as quickly as possible from the test cell to the XPS chamber, the transfer process took approximately 15 minutes, which is abundant time for reaction with air.

Air reduction of the oxide can also be used to understand the dependence of  $\text{UO}_3 \cdot (2\text{H}_2\text{O})$  vs  $\text{UO}_2$  content of the oxides on pH and Nb concentration. In all cases, potentiodynamic polarization data suggest that  $\text{UO}_3 \cdot (2\text{H}_2\text{O})$  formation occurred. If air reduction of  $\text{UO}_3 \cdot (2\text{H}_2\text{O})$  was primarily responsible for the presence of  $\text{UO}_2$  in the oxide, it is expected that highly-protective oxides with more Nb, where the path for oxygen to react with  $\text{UO}_3 \cdot (2\text{H}_2\text{O})$  is more tortuous, would be least affected. Also, for a given oxide chemistry and structure, thicker oxides should be reduced to a lesser extent than thinner oxides for a constant air exposure time. Figure 9 shows that the U in oxides that were protective and had a high Nb content (e.g., U-8Nb, pH 10.7), was predominantly in the form of  $\text{UO}_3 \cdot (2\text{H}_2\text{O})$ . Note that for protective oxides with low Nb content (e.g., U-2Nb, pH 10.7), lesser amounts of  $\text{UO}_3 \cdot (2\text{H}_2\text{O})$  were observed. Further evidence for air reduction of  $\text{UO}_3 \cdot (2\text{H}_2\text{O})$  is given by the non-protective, oxide grown on U-2Nb in pH 4 solution. Table II shows that the oxide formed during a 2-hour polarization, which was thicker, contained more  $\text{UO}_3 \cdot (2\text{H}_2\text{O})$  than the thinner one formed during a 1-hour polarization.

Figure 6 shows that although Nb promoted passivity of U-Nb alloys in acidic and neutral solutions, it had little effect in alkaline solutions. In both of the alkaline solutions examined, U-8Nb had the lowest anodic limiting current densities. In neutral and acidic solutions, Nb always had the lowest anodic limiting current densities. This behavior suggests a synergy between U and Nb and may be explained by the unique phase structure of U-8Nb. The structure of U-Nb alloys depends on Nb concentration. For U-2Nb, the structure is a distortion of the orthorhombic  $\alpha$  phase. At high temperatures, U exists in the bcc  $\gamma$  phase, and the U-8Nb structure is a distortion of the  $\gamma$  phase.

Bullock hypothesized that the room-temperature corrosion rate of the  $\gamma$  phase of U, if it could be prepared, would be inherently lower than that of the  $\alpha$  phase (8). That hypothesis, however, was based on linear extrapolations of highly-alloyed U to zero percent alloy addition, and it is not likely that the corrosion behavior would be linear as alloy additions approached zero. Still, the U-8Nb results presented here show the oxide that forms on the distorted  $\gamma$ -phase alloy in basic solutions has improved passivity over U or Nb in basic solutions. XPS analysis showed no new oxide compounds were formed. It is likely that the oxide formed on the distorted  $\gamma$ -phase was unique and was responsible for the observed behavior. However, the exact origin of the oxide behavior (crystal structure, defect structure, ordering, etc.) is not known.

DRAFT

11/12

In summary, this work has shown that electrochemically-grown oxides on U-Nb alloys (2-8 wt. % Nb) were mixed and consisted of varying amounts of  $\text{Nb}_2\text{O}_5$ ,  $\text{UO}_3 \cdot 2\text{H}_2\text{O}$ , and  $\text{UO}_2$ . The presence of  $\text{UO}_2$  was likely due to reduction of  $\text{UO}_3 \cdot 2\text{H}_2\text{O}$  in air. The results suggest that Nb additions enhanced passivity of U in acidic and neutral solutions through the formation of  $\text{Nb}_2\text{O}_5$  and, in some cases, enrichment of  $\text{Nb}_2\text{O}_5$  in the oxide. In highly acidic solutions, U dissolved actively, and Nb additions greater than 8 wt. % would be required to achieve passivity. In alkaline solutions Nb did not significantly increase the corrosion resistance of the mixed oxide, except in the case of U-8Nb where a synergistic effect, likely due to the U-8Nb phase structure, was observed. In highly alkaline solutions, Nb formed a non-protective oxide and was an ineffective alloy element for promoting passivity.

### ACKNOWLEDGMENTS

Los Alamos National Laboratory is operated by the University of California for the US Department of Energy under Contract W7405-ENG36.

### REFERENCES

- [1] N. J. Magnani, "The Reaction of Uranium and Its Alloys with Water Vapor at Low Temperatures," Sandia Laboratories Report, SAND-74-0145, Aug., 1974.
- [2] J. W. McWhirter and J. E. Draley, "Aqueous Corrosion of Uranium and Alloys: Survey of Project Literature," Argonne National Laboratory Report, ANL-4862, May, 1952.
- [3] J. L. Cadden, N. C. Jessen, and P. S. Lewis, in *Physical Metallurgy of Uranium Alloys*, J. J. Burke, D. A. Colling, A. E. Gorum, and J. Greenspan, Eds., pp. 3-81, Brook Hill Publishing Co., Chestnut Hill, MA (1976).
- [4] R. A. Vandermeer, in *Metallurgical Technology of Uranium and Uranium Alloys, Volume 1: Physical Metallurgy of Uranium and Uranium Alloys*, R. A. Vandermeer, Ed., pp. 1-45, ASM / Publishers Choice Book Mfg. Co., Mars, PA (1982).
- [5] W. L. Manner, J. A. Lloyd, R. J. Hanrahan, and M. T. Paffett, *Appl. Surf. Sci.*, **150**, 73-88 (1999).
- [6] G. C. Allen, P. M. Tucker, and J. W. Tyler, *J. Phys. Chem.*, **86**, 224-228 (1982).
- [7] M. Pourbaix, *Atlas of Electrochemical Equilibria*. Houston, TX: NACE (1974).
- [8] J. S. Bullock, in *Physical Metallurgy of Uranium Alloys*, J. J. Burke, D. A. Colling, A. E. Gorum, and J. Greenspan, Eds., pp. 847-895, Brook Hill Publishing Co., Chestnut Hill, MA (1976).